Diagnosis of Regional Monthly Anomalies Using the Adjoint Method. Part I: Temperature

ANDREW W. ROBERTSON

Meteorologisches Institut der Universität München, Munich, Germany

(Manuscript received 23 January 1991, in final form 26 June 1991)

ABSTRACT

A one-layer, tropospherically averaged tracer model and its adjoint are used to examine observed midlatitude regional anomalies in terms of horizontal advection, and the effects of adiabatic and diabatic heat sources. The adjoint of the tracer model defines an information variable that is used to trace the airmass history of central European anomalies using observed winds. Together with a history of the tracer model's heat sources and sinks, which is also derived from observations, the adjoint integration enables the effects of heat sources and advection to be quantified, using the information tracer as a weighting function. Large January temperature anomalies are found to be primarily accounted for by horizontal advection of air masses already present on 1 January, with anomalous heating/cooling during the month playing a secondary role. Quasigeostrophic theory suggests that the small heating effects implied by the one-layer model are often associated with compensation between diabatic and adiabatic heating effects, the latter accompanying vertical motions. An attempt is made to interpret these compensating heat sources and sinks in terms of the positions of the storm tracks.

1. Introduction

The present generation of climate models is unable to reach a consensus on the regional effects of a doubling of the effective CO_2 concentration in the atmosphere (Grotch and MacCracken 1991). In order to extend the predictive capability of climate models to the regional scale ($\sim$1000 km), the development of simple tools to diagnose regional climate anomalies arising in general circulation model (GCM) experiments is an important task. In particular, a diagnostic capable of discerning between the effects of anomalous advection on a given region and the effects of local as well as remote diabatic forcing would be of great interest. For instance, an anomaly in the temperature budget over Europe might be directly affected by anomalous diabatic heating accompanying sea surface temperature anomalies over the Atlantic, or it might, rather, be the product of the associated anomalous circulation pattern (or both).

The tracer model offers an obvious way of describing the evolution of an atmospheric variable in terms of its advection and (diabatic) sources and sinks, and yields particular insight if a quasi-conservative variable such as temperature is chosen. It suggests a potential diagnostic for regional anomalies. By making visible the "internal" dynamics of a regional anomaly (as if a dye tracer were injected into the flow), the tracer model has the potential to set a regional anomaly within a larger geographical context and to help identify the advective and diabatic processes responsible for maintaining it. Of course, anomalous diabatic processes will generally result in an anomalous circulation pattern so that the two are linked. Nevertheless, we will concentrate here on the linear problem and consider the independent effects of advection and sources and sinks on regional anomalies.

A very promising and novel method of *quantifying* a regional anomaly in terms of the advection of a tracer and its sources and sinks is the adjoint method as formulated by Marchuk (1974). Marchuk and Skiba (1976) have applied the method to the problem of long-range forecasting, but it lends itself ideally to the diagnostic case where all terms in the tracer equation are, in principle, known. By integrating the adjoint tracer model backwards in time, one can trace regional anomalies back to thermodynamic sources and sinks, and to an initial field. Although one generally needs to know the sources and sinks, one can estimate them as residuals from the tracer model equation itself. This procedure provides the "optimal" forcing required to make the tracer model fit the data and gives an indication about the validity of the model.

In order for such a model to be useful, it must be sophisticated enough to resolve the relevant advection and have physically meaningful sources and sinks, but be simple enough to be easily applicable. Tropospherically averaged temperature is an immediately relevant climatic variable, which could be examined by means of a simple hemispheric one-layer adjoint tracer model. The tropospheric average is convenient because vertical

Corresponding author address: Andrew W. Robertson, Dept. of Atmospheric Sciences, University of California, 405 Hilgard Ave., Los Angeles, CA 90024-1565.

advection of temperature across the tropopause is small, so that temperature advection out of the model domain is negligible if we use a hemispheric model. The attendant disadvantage is that tropospheric-average vertical motion effects become an additional thermodynamic source term, but the simplicity of the one-layer model must outweigh this problem in a first application of the method. Although linear theory suggests that, in middle latitudes, diabatic heat sources are primarily balanced by horizontal advection (the so-called "advective limit"; e.g., Smagorinsky 1953; Hoskins and Karoly 1981), with vertical motions playing a secondary role, our results do not support this hypothesis for tropospheric averages.

The aim of this paper is to illustrate the application of the adjoint method to diagnosing observed European January tropospheric temperature anomalies using a one-layer tracer model. At the same time, we examine the degree to which a one-layer model can illuminate the thermodynamics of such anomalies, and the potential of the method for use as a simple tool to investigate regional aspects of GCM climate-change experiments.

We present the model and the adjoint method in section 2 and the dataset used in section 3. The suitability of the one-layer model is checked a priori in section 4 by integrating the unforced tracer model forward in time and checking against observations. We then present an adjoint integration of the model. A prerequisite to application of Marchuk's adjoint method is an understanding of the "forcing" term (i.e., all the source, sink, and transport terms not explicitly represented by the one-layer model), which we compute as a residual of the model itself applied to observations and examine in section 5 with the aid of simple quasigeostrophic theory. Section 6 describes preliminary applications of the adjoint method to European (and other) temperature anomalies, investigating sensitivity to dissipation, length of period considered, and horizontal resolution. In section 7, we attempt a diagnosis of six Januarys over central Europe in terms of horizontal temperature advection and thermodynamic sources and sinks, considering the grand mean and anomalies defined therefrom. A discussion follows in section 8.

2. The adjoint method

This section describes the adjoint method that Marchuk (1974) originally formulated to make long-range forecasts of regional temperature (see also Kontarev 1980), but that we apply to the diagnostic problem. We assume that the regional temperature variations that interest us are described meaningfully by the simple one-layer advection model:

$$\partial T/\partial t + \mathbf{v}\cdot\nabla T + \kappa\nabla^4 T = F, \qquad (1)$$

where T is temperature and $\mathbf{v}$ is the wind velocity, both taken to be some vertical average. Here, κ is the (∇^4) horizontal diffusion coefficient and F is the "residual forcing," made up of all terms in the forecast equation for T not included on the lhs of (1): most notably diabatic effects and terms associated with vertical motions. Our aim is to diagnose the average temperature in a region G (of area $a = |G|$) in a time interval I, where $|I| = \Delta t = t_1 - t_0$

$$\overline{T}^{G,I} = \frac{1}{|G|\,\Delta t}\int_G\int_{t_0}^{t_1} T dt da \qquad (2)$$

using (1).

We first define the usual inner product of two space–time temperature vectors (T and T') belonging to the Hilbert space of all possible temperature vectors as

$$(T, T')_{D\times I} = \int_{t_0}^{t_1}\int_D TT' da dt,$$

where D is the spatial domain over which (1) is integrated. In practice, we will be considering the hemispheric domain, and T and T' will be spectral expansions. The inner product is then easily computed via the transform method in gridpoint space, as detailed in the Appendix. If A represents an operator transforming the vector function T into another vector function within the same Hilbert space, then the adjoint of A is defined by A^*, such that the Green's identity

$$(T', AT)_{D\times I} = (A^*T', T)_{D\times I}$$

is satisfied (e.g., Lanczos 1961).

We now specify A to be the linear differential operator representing the lhs of (1), remembering that $\mathbf{v}$ is prescribed, and proceed to determine its adjoint. Noting that the adjoint of a sum is the sum of the adjoints, integrating each individual term by parts (e.g., Kontarev 1980) shows that the adjoint corresponding to (1) is

$$-\partial T^*/\partial t - \mathbf{v}\cdot\nabla T^* + \kappa\nabla^4 T^* = F^*, \qquad (3)$$

where T^* is the adjoint variable and F^* is some arbitrary conjugate forcing function to be specified. Effectively, T^* is advected backward in time from t_1 to t_0 with the wind reversed in sign, but the diffusion term still acts in the correct sense. We now take the inner product of (1) with T^* and (3) with T and subtract the second from the first, yielding:

$$\left(T^*, \frac{\partial T}{\partial t}\right)_{D\times I} + \left(T, \frac{\partial T^*}{\partial t}\right)_{D\times I} = (T^*, F)_{D\times I} - (T, F^*)_{D\times I}, \qquad (4)$$

where we have assumed

$$\nabla\cdot\mathbf{v} = 0.$$

The diffusion term vanishes in (4) if the domain D has periodic boundary conditions (as in the case of the

hemisphere), because integrating by parts gives in this case

$$\int_D \int_{t_0}^{t_1} (T^* \kappa \nabla^4 T - T \kappa \nabla^4 T^*) dt da$$

$$= \kappa \int_D \int_{t_0}^{t_1} \{\nabla \cdot (T^* \nabla^3 T - T \nabla^3 T^* - \nabla T^* \nabla^2 T + \nabla T \nabla^2 T^*)\} dt da = 0.$$

In the adiabatic case $F = F^* = 0$, (4) gives

$$\int_D \int_{t_0}^{t_1} \left(T^* \frac{\partial T}{\partial t} + T \frac{\partial T^*}{\partial t} \right) dt da = \int_D [T T^*]_{t_0}^{t_1} da$$

$$= \int_D (T_1 T_1^* - T_0 T_0^*) da = 0,$$

where T_1 denotes T at $t = t_1$, etc. The particular choice

$$T_1^* = T_1$$

yields

$$\int_D T_1^2 da = \int_D T_0 T_0^* da. \tag{5}$$

Note that this is independent of the presence of dissipation, whose effects are included in both T_1 and T_0^*. In the absence of dissipation, the conservation of heat implies that all moments of the T distribution are conserved, so that we must have $T_0^* = T_0$. With these boundary conditions, (1) and (3) satisfy the Green's identity so that we have precisely defined the adjoint problem, whose solution is in fact exactly the same as the initial data of the direct problem (1) (Kontarev 1980).

In the diabatic case, (4) yields

$$\int_D (T_1 T_1^* - T_0 T_0^*) da = \int_D \int_{t_0}^{t_1} (T^* F - T F^*) dt da. \tag{6}$$

We now choose

$$T_1^* = 0 \tag{7}$$

as initial condition for the adjoint problem and define the conjugate forcing function *locally* over the "target area" G during the time interval I, such that

$$F^* = \begin{cases} \dfrac{1}{|G| \Delta t}, & \text{for } x, y \in G \text{ and } t \in I \\ 0, & \text{for } x, y \notin G \text{ or } t \notin I \end{cases}, \tag{8}$$

so that F^* is a step function that singles out the domain (G, I), and

$$\int_D \int_{t_0}^{t_1} T F^* dt da = \frac{1}{|G| \Delta t} \int_G \int_{t_0}^{t_1} T dt da = \overline{T}^{G,I}. \tag{9}$$

Thus, (6) becomes

$$\overline{T}^{G,I} = \int_D T_0 T_0^* da + \int_D \int_{t_0}^{t_1} T^* F dt da. \tag{10}$$

This is the central equation of Marchuk's adjoint method and states that the average temperature over region G during the interval I, $\overline{T}^{G,I}$ depends on the temperature field throughout the domain at time $t = t_0$ (the "initial conditions") and the forcing within the time interval I throughout the domain. The importance of each field is weighted by the "influence function" T^*, which is obtained by integrating the adjoint tracer equation (3) backward using (7), together with prescribed winds. The influence function T^* is a positive quantity that has the sense of an information density, with F^* being a local information source. Note how the adjoint boundary conditions enter into (10) and are crucial in defining the adjoint problem. In contrast to the conditions (5), the Green's identity is now only satisfied with the addition of a boundary term (the initial conditions); this constitutes the so-called extended Green's identity.

Equation (10) may easily be extended to consider the effect of F at times before the onset of the regional feature of interest, by defining F^* for a target space–time interval analogous to (8). In this way, the initial-conditions term may be expressed in terms of $F(t < t_0)$. The forcing term itself may be further divided into contributions from different zones D_i, such that

$$\int_D \int_{t_0}^{t_1} T^* F dt da = \sum_i \int_{Di} \int_{t_0}^{t_1} T^* F dt da,$$

with $D = \sum_i D_i$, allowing the influence of each zone on the target area G to be estimated.

It is useful to define the temperature in (10) relative to some reference or basic temperature value (T_b) as $T' = T - T_b$, so that the regional temperature anomaly is given by

$$\overline{T}'^{G,I} = \overline{T}^{G,I} - T_b, \tag{11a}$$

and to define

$$T_b = \overline{\hat{T}}^{G} = \int_D \hat{T} F^* da, \tag{11b}$$

where the hat denotes a climatological average. The anomaly form of (10) is then given by

$$\boxed{\overline{T}'^{G,I} = \int_D (T_0 - T_b) T_0^* da + \int_D \int_{t_0}^{t_1} T^* F dt da} \tag{12}$$

where the initial-conditions term now describes sources of relatively warm or cold air. Note that the rhs of (12) still contains a climatological component associated with $\hat{T}^*$, and $\hat{F}$. In section 7, we will remove this com-

ponent by examining the deviations of the terms on the rhs of (12) from their climatological values.

The application of (12) requires F to be specified, but it may also be computed optimally from (1) as a residual, so that (12) is exactly satisfied. Obvious error "sinks" in the spatial distribution of $\overline{F}^t$ computed via (1) can identify regions where the model is poor, although the error sinks in F may partially cancel errors in T^* in the integrals in (12).

Discrete spectral models of (1) and its adjoint (3) have been constructed on the hemisphere. The transform method is used to evaluate the advection term, with a leapfrog scheme for the time integration, initialized with a forward Euler step. The adjoint model is identical to the direct (forward) version, except that it is integrated backward in time with the (prescribed) advecting winds reversed in sign. Talagrand and Courtier (1988) have shown that for the pseudospectral

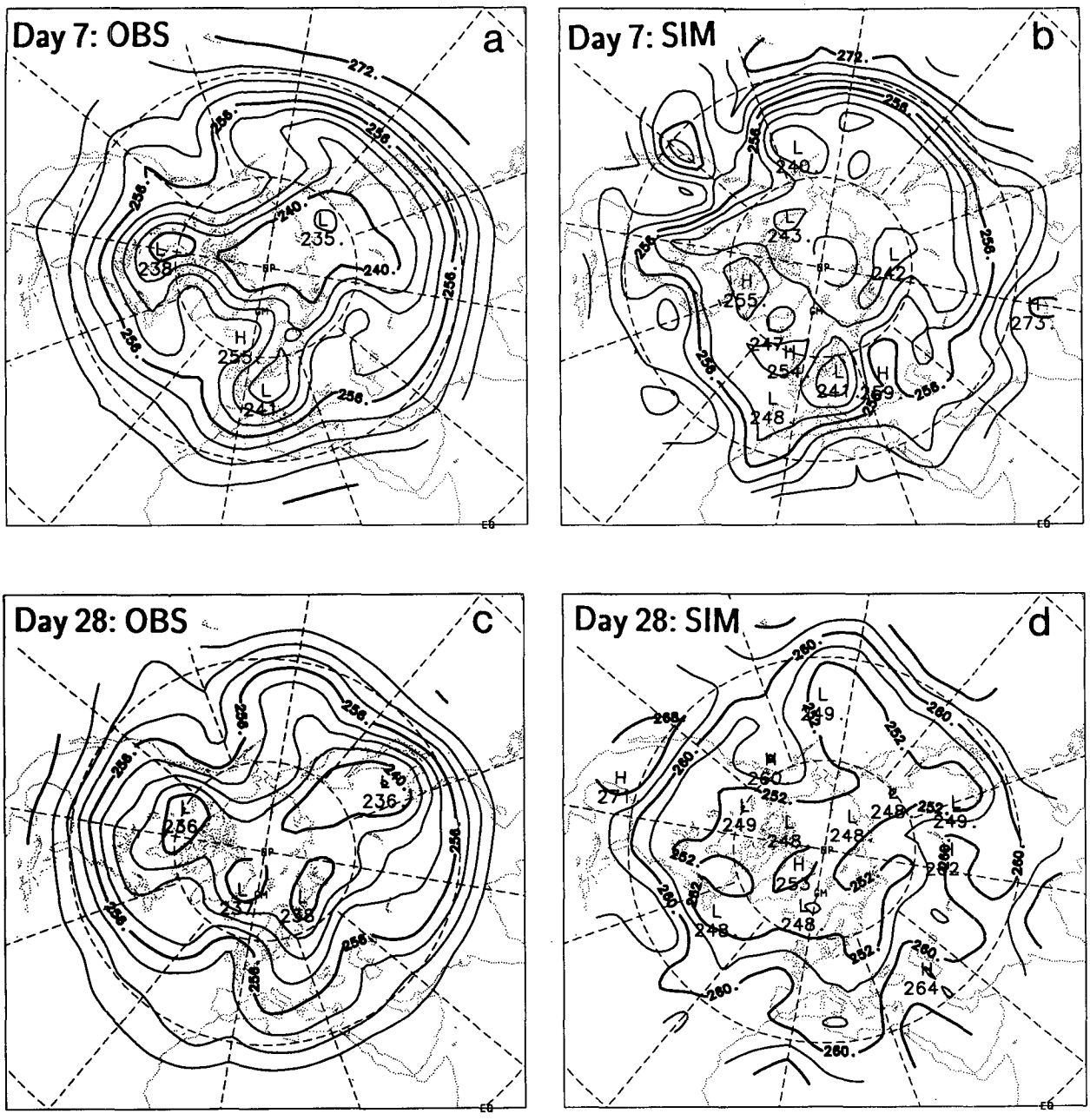

FIG. 1. Direct unforced integration of (1) starting from observed $\langle T \rangle$ at 0000 UTC 1 January 1985. Day 7: (a) observed $\langle T \rangle$, (b) simulation. Day 28: (c) observed $\langle T \rangle$, (d) simulation. Contour interval 4 K. All maps are polar stereographic projection with Greenwich meridian bottom left center.

model, the adjoint of the unaliased discretized analog of a linear operator is precisely the unaliased discretized analog of its adjoint. They also prove that the adjoint of the leapfrog time-differencing scheme amounts to a mere change of sign, but that, strictly speaking, a modified final step (the adjoint of the forward Euler step) is required.

The discretized form of (12) is derived in the Appendix. Unless stated otherwise, we use a triangular truncation at total wavenumber $n = 21$ (T21), a dissipation time scale of $T_D = 1$ day at $n = 21$, and a one-hour time step. Although the finite spectral representation means we cannot enforce the positivism of T^*, the hemispheric mean of the spectral problem (the $n = 0$ component) is trivial and arbitrary, so that negative values pose no fundamental difficulty. In practice, the above dissipation largely precludes negative values in the 1-month integrations considered below.

3. The dataset

Temperature, rotational wind, and vertical velocity taken from six winters (1979/80–1984/85) of daily (0000 UTC) data from the European Centre for Medium-Range Weather Forecasts (ECMWF) are used in this study. The data is Northern Hemispheric and truncated at T42, of which we mainly employ the T21 subset. Each winter comprises 110 days, starting on 20 November, and we use the data levels 850, 700, 500, and 300 mb, defining (1), (3), and (12) in terms of tropospheric averages given by

$$\langle x \rangle \equiv \frac{1}{4}(x_{850} + x_{700} + x_{500} + x_{300\text{mb}})$$

for each variable. The angle brackets are generally omitted in the following, but they are implied throughout.

The data are interpolated between days using cubic splines, to be available at each time step of the model. Linear temporal interpolation turns out to give almost indistinguishable results.

4. Forward and adjoint integration of the tracer model

We can get some idea of the importance of the forcing F by integrating (1) with $F = 0$ and $\mathbf{v}$ prescribed from observations. Figure 1 illustrates a comparison with observations after 7 and 28 days, starting from the observed temperature distribution at 0000 UTC 1 January 1985. Because the wind is prescribed at each time step, the phases of the troughs are never lost, even after 28 days. However, the model is unable to maintain the wave amplitudes, and there is an increase in small-scale features, which worsens if the dissipation strength is reduced. After 28 days meridional gradients become very weak and the pole warms by some 15 K, consistent with northward heat transport and mixing (dissipation) in the absence of diabatic forcing. Obviously, F is important, but the experiment demonstrates that interpolating the advecting wind from once-daily values gives a plausible simulation.

We now perform an adjoint integration in which (3) is integrated backward for 31 days, starting at t_1 = 2400 UTC 31 January 1985, with $T_1^* = 0$ as initial condition. The integration is forced by including a constant information source F^* given by (8) of unit information-density amplitude per day [$F^* = 1/(\Delta t|G|) = 1$ IDU day^{-1}, where IDU stands for (arbitrary) "information-density unit"], whose form is illustrated in Fig. 2. This conjugate forcing function was constructed on the model's transform grid to be a longitude–latitude rectangular maximum over central Europe, quickly becoming zero elsewhere, and then truncated to T21—hence the rounded profile seen in Fig. 2. During the first 8 days of integration (Fig. 3a), the information tracer T^* increases locally and is advected to the west by the adjoint wind in a burstlike fashion. The dissipation is strong enough to rather rapidly dissipate the structures that are advected away from the source region, and to avoid significant negative values. During the last eight days (Fig. 3b), T^* is strong over the source region and is advected to the north and east, consistent with the presence of a blocking ridge over the east Atlantic during this period. Note that because $F^*(t) = \text{const}$, the information tracer remains strong over the source region, even up to time $t = t_0$.

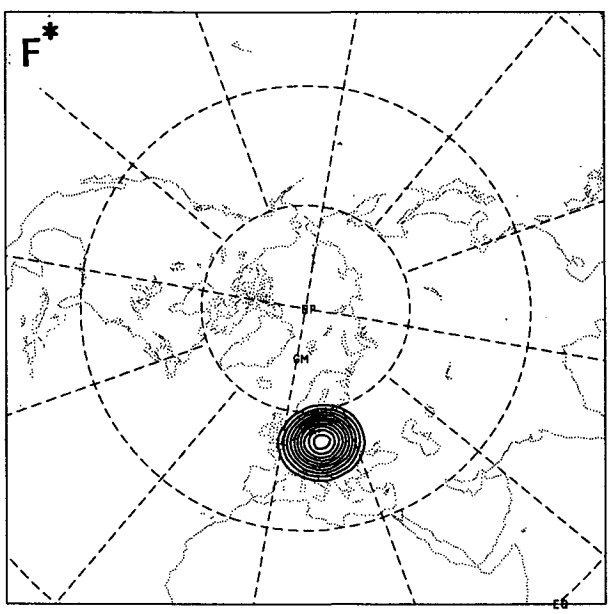

FIG. 2. Conjugate forcing function, F^*, situated over central Europe truncated at T21, of unit amplitude per day. Contour interval 0.1 IDU day^{-1} (IDU stands for "information-density unit" and is arbitrary); zero contour omitted.

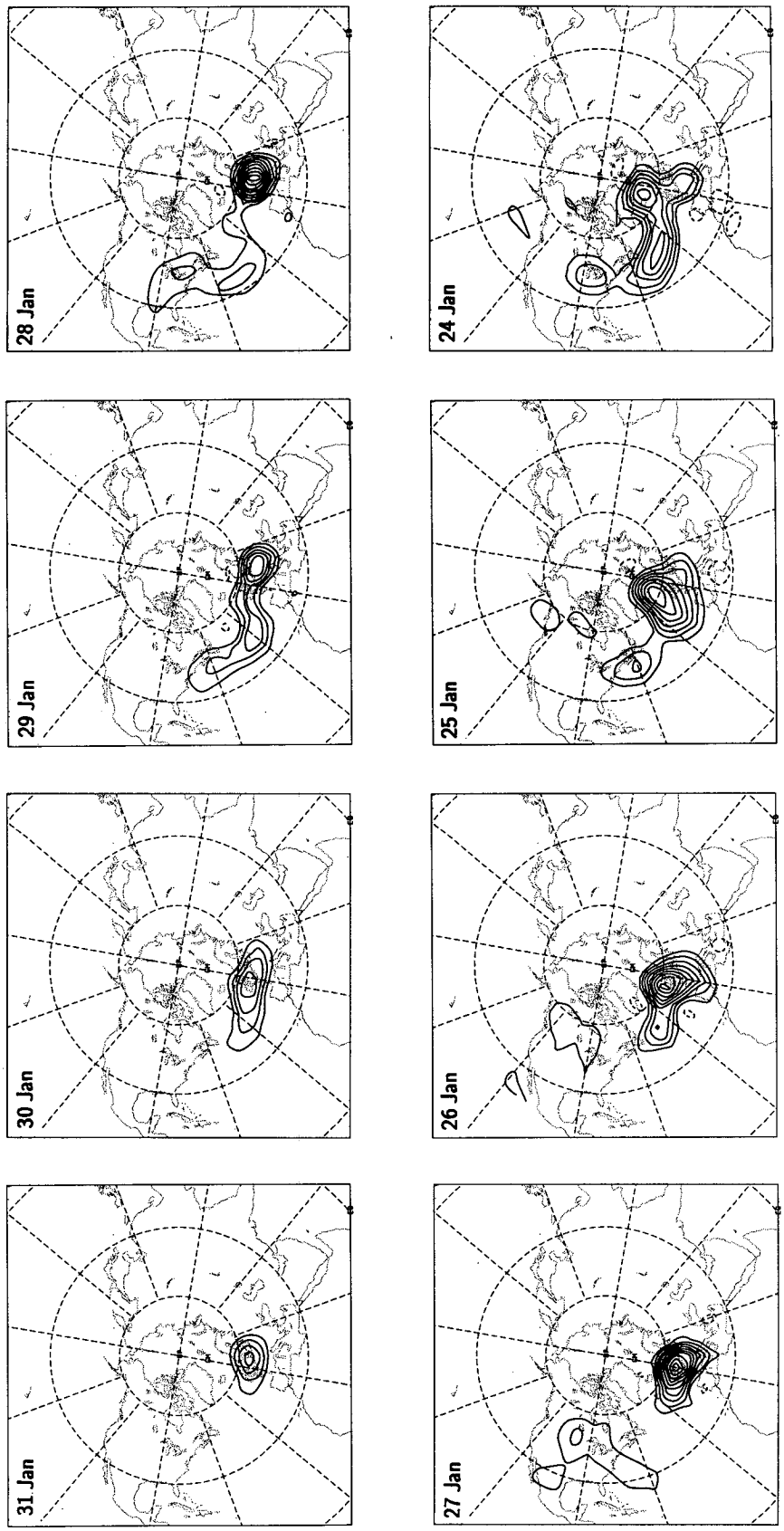

FIG. 3. Daily evolution of T^* from adjoint integration forced by F^* in Fig. 2 held constant in time, starting at time t_1 = 2400 UTC 31 January 1985 with $T_1^* = 0$.
(a) First 8 days, (b) last 8 days of integration. Contour interval 1 IDU; zero contour omitted.

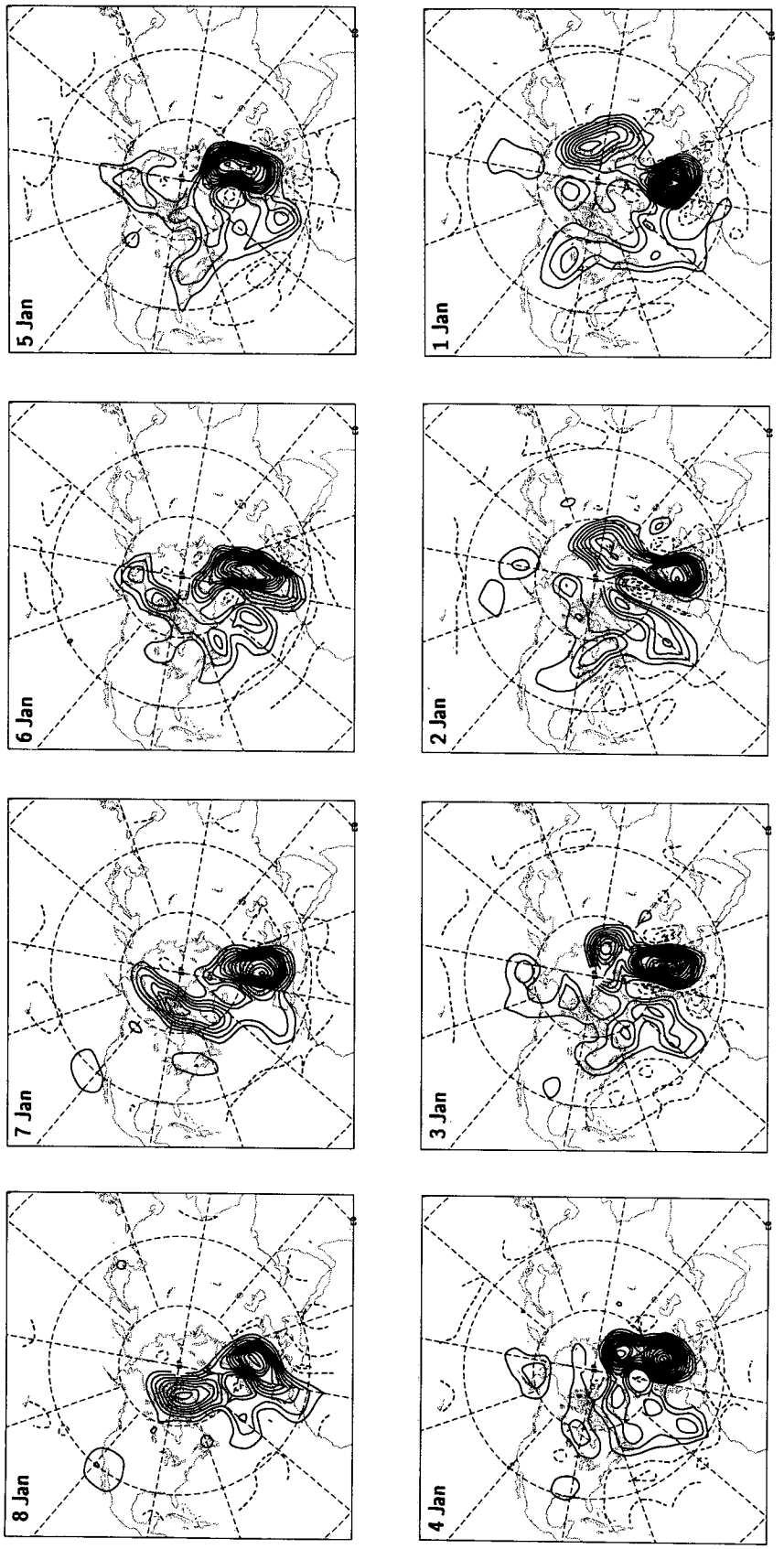

FIG. 3. (*Continued*)

At t_0 = 0000 UTC 1 January 1985 the information tracer indicates that the air reaching the target region during the month had roots over Siberia, Europe, Canada, and the Atlantic. Using the temperature distribution at $t = t_0$ (T_0), one could classify these airmass origins by temperature. However, one also needs to know the history of the model's heat sources and sinks during the course of the month (i.e., the forcing term), in order to link the air history with the regional temperature anomaly via (12).

5. The residual forcing

The six-January mean residual forcing $\hat{F}$ (where the caret denotes the six-January grand mean), computed as a residual of (1) using the same dissipation and numerical scheme as in the adjoint integration, is shown in Fig. 4a. The effect of the dissipation is very small and in the long-term average, local tendencies are negligible so that $\hat{F}$ essentially represents the climatological horizontal advection. Splitting $\hat{F}$ into transient eddy

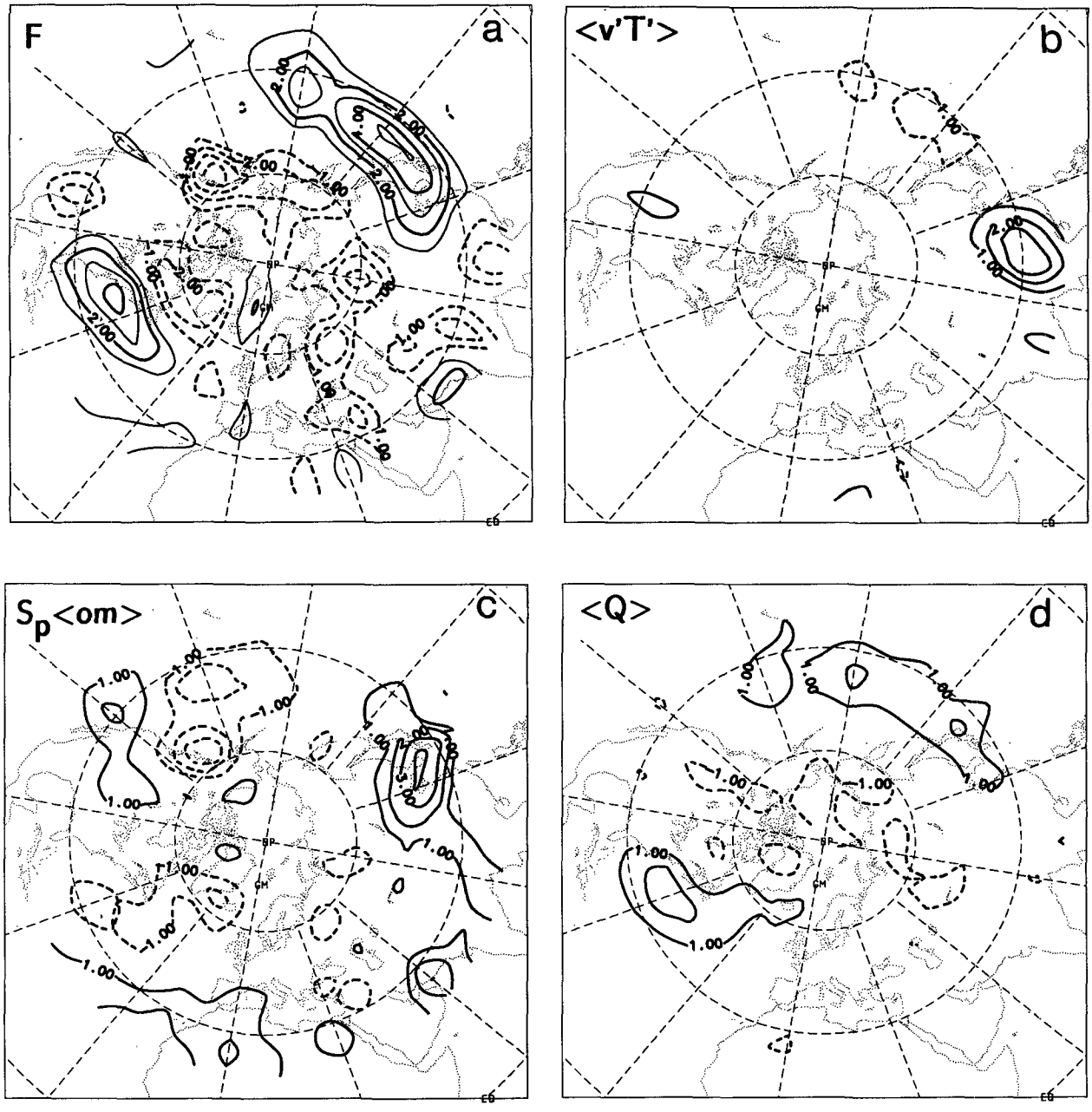

FIG. 4. Six-January means: (a) $\hat{F}$, (b) $\langle\widehat{v'T'}\rangle$, (c) $S_p\langle\hat{\omega}\rangle$ and (d) $\langle\hat{Q}\rangle$. Contour interval of 1 K day^{-1}; zero contour omitted. S_p = 0.06 K mb^{-1}.

and stationary wave components suggests that the latter generally dominate, but that eddies are important over the west Atlantic sector.

If the atmosphere were to approach the "advective limit" where diabatic heating is balanced purely by horizontal motions, then Fig. 4a could be interpreted in terms of diabatic effects. The two maxima in $\hat{F}$ off the east coasts of the continents would then correspond to diabatic heat sources balanced by cold advection, with diabatic cooling over the northern oceans balanced by poleward warm advection. To investigate the validity of this picture, we have estimated the effects of vertical motions implied by quasigeostrophic theory. The thermodynamic equation in the quasigeostrophic approximation reads (e.g., Holton 1979):

$$\partial T/\partial t + \mathbf{v}\cdot\nabla T - S_p\omega = Q,$$

where Q is the diabatic temperature tendency and $S_p \equiv -T\partial \ln\theta/\partial p$ is the static stability, which is taken to be a constant (θ is potential temperature). Taking the tropospheric average $\langle\ \rangle$ defined in section 3 yields [analogous to (1)]

$$\partial\langle T\rangle/\partial t + \langle\mathbf{v}\rangle\cdot\nabla\langle T\rangle = F,$$

where

$$F = \langle Q\rangle + S_p\langle\omega\rangle - \langle\mathbf{v}'\cdot\nabla T'\rangle, \qquad (13)$$

and the prime denotes a deviation from the tropospheric average, so that $\langle Q\rangle$ can be estimated as a residual.

Panels (b), (c), and (d) of Fig. 4 illustrate, respectively, $\langle\widehat{\mathbf{v}'\cdot\nabla T'}\rangle$, $S_p\langle\hat{\omega}\rangle$, and the residual $\langle\hat{Q}\rangle$ (where the hat again denotes the six-January grand mean), taking $S_p \sim 0.06$ K mb^{-1}. The cross-correlation term (which is computed daily and then time averaged) has a dipole structure over China/Japan that accounts for the negative pole in $\hat{F}$ over China, and part of the amplitude of the downstream positive pole. Elsewhere, this term is small. The positive pole in $(\hat{F} - \langle\widehat{\mathbf{v}'\cdot\nabla T'}\rangle)$ (not shown) over Japan is accounted for largely by the adiabatic term, suggesting a balance between orographically forced descent downstream of the Tibetan plateau and westerly cold advection. The adiabatic term also has the characteristic orographically forced signature up- and downstream of the Rockies, and indicates ascent over the oceans. The spatial distribution of the diabatic heating implied by quasigeostrophic theory (Fig. 4d) exhibits two distinct maxima of $\sim$2 K d^{-1} over the oceans, whose positions coincide with the storm tracks. Indeed, Fig. 4d compares well with column-averaged diabatic heating computed from observations by Hoskins et al. (1989), demonstrating the utility of quasigeostrophic theory, despite neglect of the eddy vertical motions, and indicating that our choice of S_p is reasonable. Comparing Figs. 4a and 4d, it is certainly clear that adiabatic temperature changes associated with vertical motions are crucial and cannot be neglected in our analysis.

TABLE 1. Values of terms in (12) in kelvin for I = January 1985 as a function of the reference temperature, T_b; $\int_H$ denotes integration over the hemisphere.

T_b (K)	Anomaly $\overline{T^*}^{GJ}$	ICs $\int_H (T_0 - T_b)T_0^*$	Forcing $\int_H \int_I T^*F$
261	−12.58	−10.15	−2.45
251	−2.60	−0.15	−2.45

6. Application of the adjoint method: Preliminary experiments

a. *January 1985 over central Europe*

The adjoint model quantifies regional temperature anomalies in terms of an initial temperature distribution, together with "forcing" effects not described explicitly by the one-layer advection model. The information tracer T^* singles out initial conditions and forcing effects from their respective hemispheric distributions, which define the thermodynamics [according to (1)] of the regional anomaly.

To apply the model, we define a regional temperature anomaly over central Europe for the month of January 1985 by way of (9) and (11), with $F^* = 1$ IDU day^{-1} inside the region G as in section 4 (Fig. 2). The terms in (12) are then evaluated using T^* derived from the adjoint integration in section 4, with the forcing term F evaluated as a residual from (1) at each time step.

Table 1 gives the magnitudes of the three integrals in (12) for January 1985, scaled to degrees kelvin. Equation (12) is generally satisfied to well within ±0.01 K in all the cases examined below. In the first row of Table 1, temperatures are relative to the hemispheric mean (261 K), and the regional temperature anomaly is negative (−12.6 K). The initial-conditions term ("ICs" hereafter) largely supplies the hemispheric anomaly, and is large compared to the forcing effects. In the second row, temperatures are defined as deviations from T_b = 251 K, the six-January climatological mean temperature over the target region computed via (11b). Central Europe was thus anomalously cold in January 1985 (−2.6 K), while the ICs were almost neutral with respect to T_b, so that the (relatively) cold air derived predominantly from the forcing effects during the month.[1] Note from Table 1 how the magnitude of the ICs depends on the choice of T_b.

[1] This does not mean that there was no anomaly in the January 1985 ICs with respect to climatology. On the contrary, both F and T_0^* have climatological components, and it is shown in section 7 that the anomaly with respect to the six-January climatology is in fact primarily associated with *anomalous* ICs, with *anomalous* forcing playing a relatively minor role.

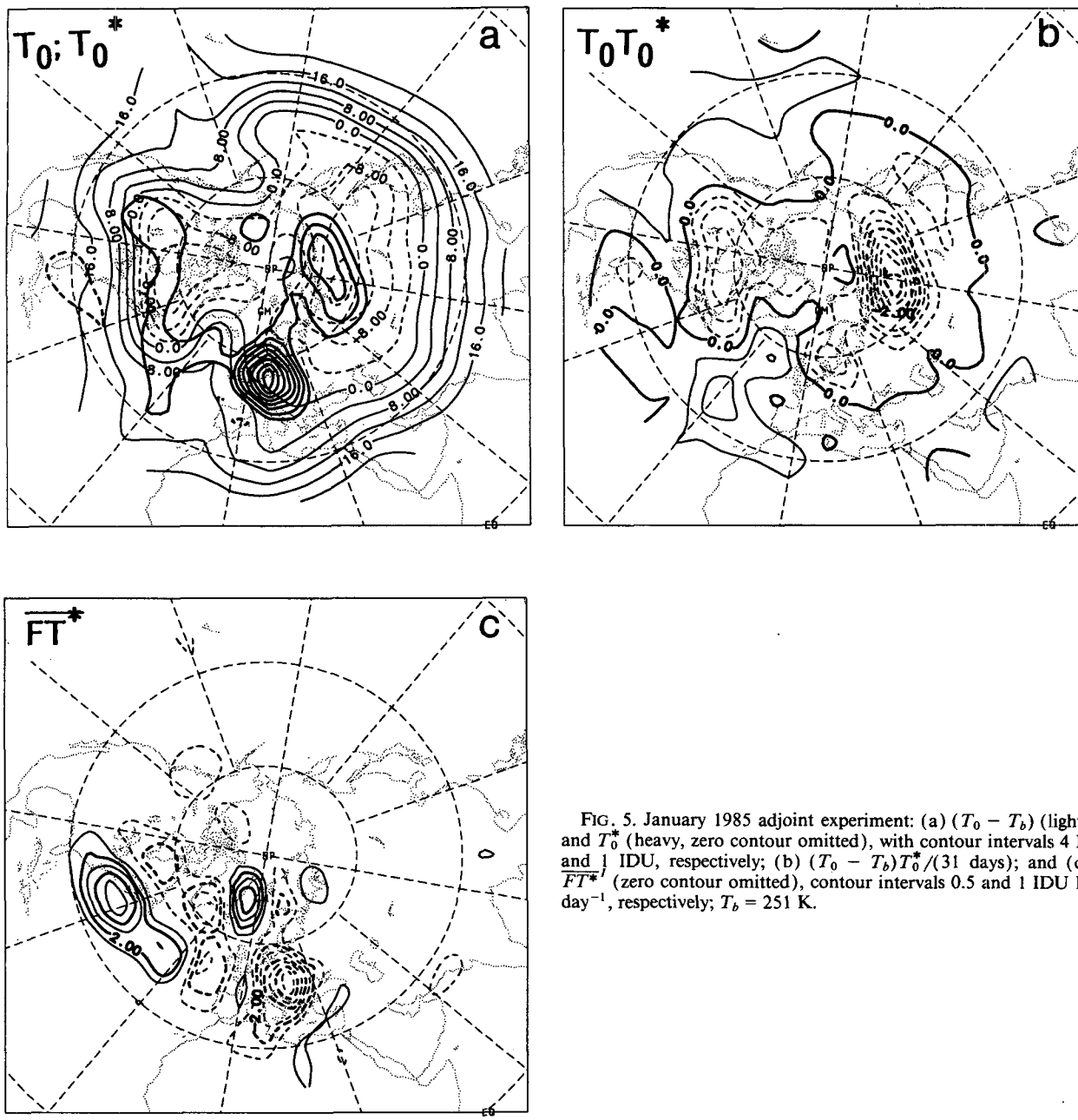

FIG. 5. January 1985 adjoint experiment: (a) $(T_0 - T_b)$ (light) and T_0^* (heavy, zero contour omitted), with contour intervals 4 K and 1 IDU, respectively; (b) $(T_0 - T_b)T_0^*/(31$ days); and (c) $\overline{FT^*}^l$ (zero contour omitted), contour intervals 0.5 and 1 IDU K day^{-1}, respectively; $T_b = 251$ K.

The thermodynamics behind the integrals in Table 1 can be examined in terms of the associated spatial fields. Figure 5a shows temperature deviations from the European January climate $(T - T_b)$ on 1 January, with the distribution of T_0^* superimposed in bold contours. The information tracer indicates the importance of preexisting cold air masses over Siberia and Canada, while the primary airmass source region, located over the target region itself, has relatively neutral temperature. The product $(T_0 - T_b)T_0^*/\Delta t$ (Fig. 5b) highlights Siberia as the most marked preexisting advective source of cold air, though Table 1 indicates that the hemispheric integral almost vanishes, so that preexisting warm air sources are just as important in Fig. 5b, if not as pronounced.

Figure 5c illustrates the contribution of net forcing effects to the anomaly, $\overline{FT^*}^l$ (i.e., the effects of diabatic and adiabatic heating during the month, together with turbulent transports and model errors). There is strong net thermodynamic forcing upstream over the Atlantic and locally over the target region itself. Regions of positive and negative forcing tend to cancel one another,

but cooling dominates according to Table 1. From section 5, we expect adiabatic effects associated with vertical motions to be significant, and this point will be taken up again in section 7. The forcing distribution emphasizes westerly advection in contrast to the ICs, which highlight easterly advection from Siberia. This underlines the temporal inhomogeneity of the month noted in Fig. 3, the spatial structure of the ICs being biased toward the circulation at the beginning of the month.

b. *The role of the dissipation*

In the adjoint integration (Fig. 3) it appeared that small outliers of T^* were often quite rapidly dissipated. In order to check that important information is not being lost, we tabulate the effect of changing the strength of the dissipation in (3) in Table 2. Increased dissipation ($t_D < 1$ day) erases memory of the initial conditions while at the same time leading to an additional error sink in F, which increases the importance of the forcing term. It also damps the influence function out more quickly away from the target region on small scales. The analysis becomes increasingly "short sighted" as the dissipation strength is increased, decreasing the sphere of influence of advection and forcing. Choosing a scale-selective dissipation is consistent with a cascade of information to smaller scales.

The integrals in Table 2 are rather insensitive to decreasing the dissipation strength beyond $t_D > 1$ day, or even to suppressing it altogether. The spatial distributions in Fig. 5 ($t_D = 1$ day) become noisier if the dissipation strength is decreased, but retain their main features. Associated with the information cascade to smaller scales, T^* frequently becomes locally negative with weak dissipation, especially at low latitudes. In order to avoid such spurious behavior of the tracer, a moderate dissipation is preferable. Its effect is essentially to confine interest to the larger spatial scales.

An additional experiment has been performed in which the advection term in (1) and (3) was set to zero, so that F just represents local tendencies plus dissipation effects. In the adjoint integration, information is diffused away from the source as a function of the dissipation strength, so that T^* has a circular pattern about the source. Suppressing advection reduces the size of the forcing integral (for a given dissipation strength) because horizontal advection and heating effects tend to balance.

TABLE 2. Values of terms in (12) in kelvin for January 1985 as a function of the dissipation time scale t_D at $n = 21$ with $T_b = 251$ K.

Dissipation t_D (day)	Anomaly $\overline{T'^{G,I}}$	ICs $\int_H (T_0 - T_b)T_0^*$	Forcing $\int_H \int_I T^*F$
0.08	−2.60	+1.81	−4.41
0.25		+1.05	−3.65
1.00		−0.15	−2.45
4.00		−0.68	−1.89
16.00		−0.62	−1.98
∞		−0.50	−2.10

TABLE 3. Values of terms in (12) in kelvin for differing Δt with $t_D = 1$ day and $T_b = 261$ K. Periods are given in text. The far-right column gives the forcing integral normalized by Δt.

Duration Δt (days)	Anomaly $\overline{T'^{G,I}}$	ICs $\int_H (T_0 - T_b)T_0^*$	Forcing $\int_H \int_I T^*F$	Forcing/Δt K day^{-1}
7	−9.00	−8.74	−0.27	−0.04
15	−8.88	−8.06	−0.82	−0.05
31	−12.60	−10.15	−2.45	−0.08
60	−10.22	−4.92	−5.31	−0.09
109	−9.90	−3.04	−6.86	−0.06

c. *Experiments with episodes of different durations*

From (12) it is clear that increasing Δt also increases the importance of the forcing effects, which act over a longer period, while dissipation further erodes memory of the initial conditions. Table 3 shows the results of experiments with $\Delta t = 7$, 15, 60, and 109 days, with $t_D = 1$ day and $T_b = 261$ K (hemispheric mean). The time periods all end at 2400 UTC 31 January 1985, except the entire 109-day winter season, which ends at 2400 UTC 7 March 1985. The contribution from the ICs clearly decreases with increasing Δt, while the importance of the forcing increases. However, the forcing normalized by Δt remains fairly constant for $\Delta t \geqslant 15$ days, although week-to-week variability has been found to give very different values for different 7-day periods.

d. *An experiment with increased horizontal resolution*

In order to test the adequacy of T21 horizontal resolution, we have repeated the January 1985 experiment with the resolution of all fields doubled to T42 (Table 4), using a model time step of 1/2 h. The rectangular step-function form of the F^* function is now much better resolved (not shown), but this has very little effect on the magnitude of the regional anomaly.

TABLE 4. Values of terms in (12) in kelvin using T42 truncation, as a function of the dissipation time scale t_D at $n = 42$. $T_b = 251$ K.

Dissipation t_D (days)	Anomlay $\overline{T'^{G,I}}$	ICs $\int_H (T_0 - T_b)T_0^*$	Forcing $\int_H \int_I T^*F$
0.07	−2.66	+0.04	−2.69
1.00		−1.27	−1.36
4.00		−1.24	−1.39

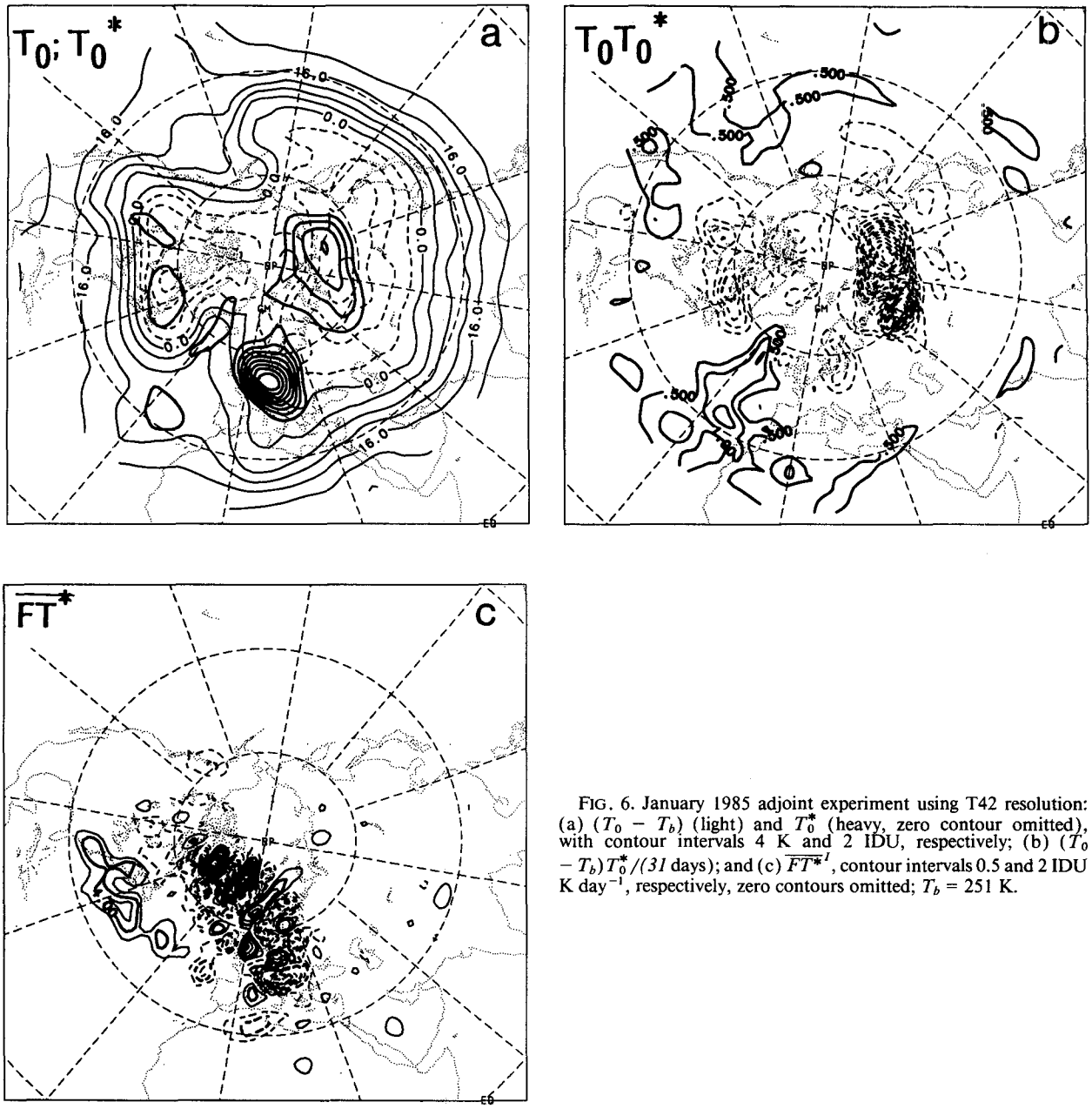

FIG. 6. January 1985 adjoint experiment using T42 resolution: (a) $(T_0 - T_b)$ (light) and T_0^* (heavy, zero contour omitted), with contour intervals 4 K and 2 IDU, respectively; (b) $(T_0 - T_b)T_0^*/(31$ days); and (c) $\overline{FT^*}^I$, contour intervals 0.5 and 2 IDU K day^{-1}, respectively, zero contours omitted; T_b = 251 K.

The high-dissipation case in Table 4 corresponds to t_D = 1 day at n = 21, which is the standard dissipation strength used in the T21 experiments, but implies a very strong dissipation at the newly resolved scales. The values of the integrals in (12) are almost identical to their T21 counterparts in this case, and the method is robust in this respect. With a weaker dissipation more suited to the higher truncation (t_D = 1 day at n = 42), the amplitude of the forcing is halved, indicating that, at high dissipation, important information of the initial state is being dissipated. Decreasing the dissipation further has little further effect on the values of the integrals.

Figure 6 illustrates the spatial fields for the t_D = 1 day, n = 42 case. Apart from the larger amplitudes and finescale structure at T42, the results are qualitatively similar to those at T21 in Fig. 5 (even though the dissipation is also much weaker). In fact, the $\overline{FT^*}^I$ field in Fig. 6c resembles its T21 counterpart very closely if it is truncated to T21. The small-scale "noodled" structure downstream of Greenland appears to be associated with orography.

TABLE 5. Values of terms in (12) in kelvin for other target regions: BI–British Isles, ECO–U.S. East Coast. T_b = 254 K.

Region	Anomaly $\overline{T'^{G,I}}$	ICs $\int_H (T_0 - T_b)T_0^*$	Forcing $\int_H \int_I T^*F$
BI	−2.25	−1.64	−0.61
ECO	−1.41	+1.90	−3.30

e. *Other target regions*

To illustrate the effect of moving the target region, we consider here two other regions during January 1985 (with T21 resolution). First, we simply shift F^* in Fig. 2 by 20° westward to lie over the British Isles (BI), to assess the sensitivity of the model to a small change in the location of the target region. Second, we center the information source over the region of implied diabatic heating over the east coast (ECO) of the United States. The values of the integrals obtained are given in Table 5, where anomalies are with respect to the climatological value $\overline{\hat{T}^{G,I}}$, which in both cases gives T_b = 254 K. Note again that as in section 6b, one cannot speak of *anomalous* ICs and forcing because of climatological components in F and T^*.

The temperature anomaly over the British Isles is similar to that over central Europe, but here, in contrast, cold air relative to T_b dominates the ICs. Nevertheless, the spatial distribution in Fig. 7 indicates that, compared to the central European case, there is less influence from Siberia and more warm Atlantic air (note that BI is climatologically warmer than central Europe by 3 K). The net cooling effects on BI (Table 5) are smaller than in the central European case, and Fig. 7b highlights the importance of heating over the BI target region itself. Note that both integrals and distributions are significantly different from their central European counterpart despite the small displacement in target region.

The fields for the ECO case are presented in Fig. 8, along with the F^* function defining the target region. A large, relatively *warm* air mass over the Gulf of Mexico dominates the ICs in Table 5. Net forcing effects (on the target region) are correspondingly large and negative, and come from as far upstream as the west Pacific. Cooling over Alaska and eastern Canada dominates over warming over the west Pacific and the target region itself. The ECO pictures strongly contrast with the European west coast situation, and highlight the method's scope to identify regions of advective influence.

7. A diagnosis of six Januarys over central Europe

In this section, we return to central Europe and use the adjoint model to compare the six Januarys of our dataset. The six-January mean is used to define *climatological* ICs and forcing terms, so that we are now able to define *anomalies* in the ICs and forcing as deviations from this mean. The six-January averages of (12) are tabulated in the first row of Table 6, with the integrals for each January expressed as deviations from this mean in the remainder of the table.

The six-January average forcing is characterized by thermodynamic cooling (~2 K mo^{-1}), and the cli-

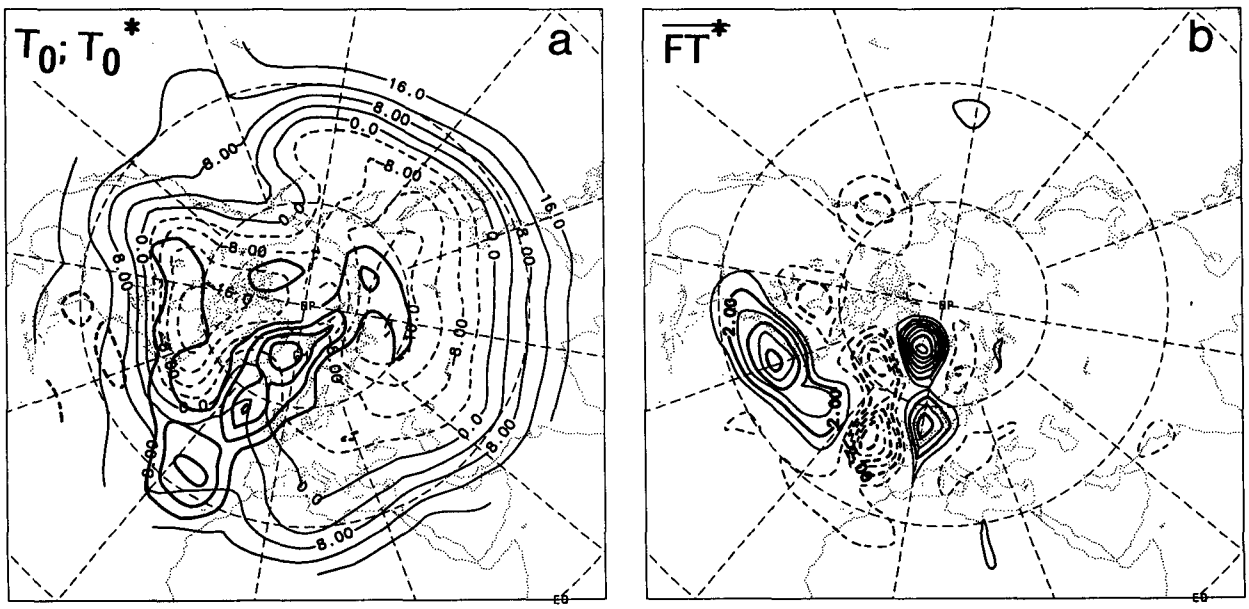

FIG. 7. BI target region (January 1985, T21): (a) $(T_0 - T_b)$ (light) and T_0^* (heavy, zero contour omitted), with contour intervals 4 K and 1 IDU, respectively; (b) $\overline{FT^*}'$, contour interval 1 IDU K day^{-1}, zero contour omitted; T_b = 254 K.

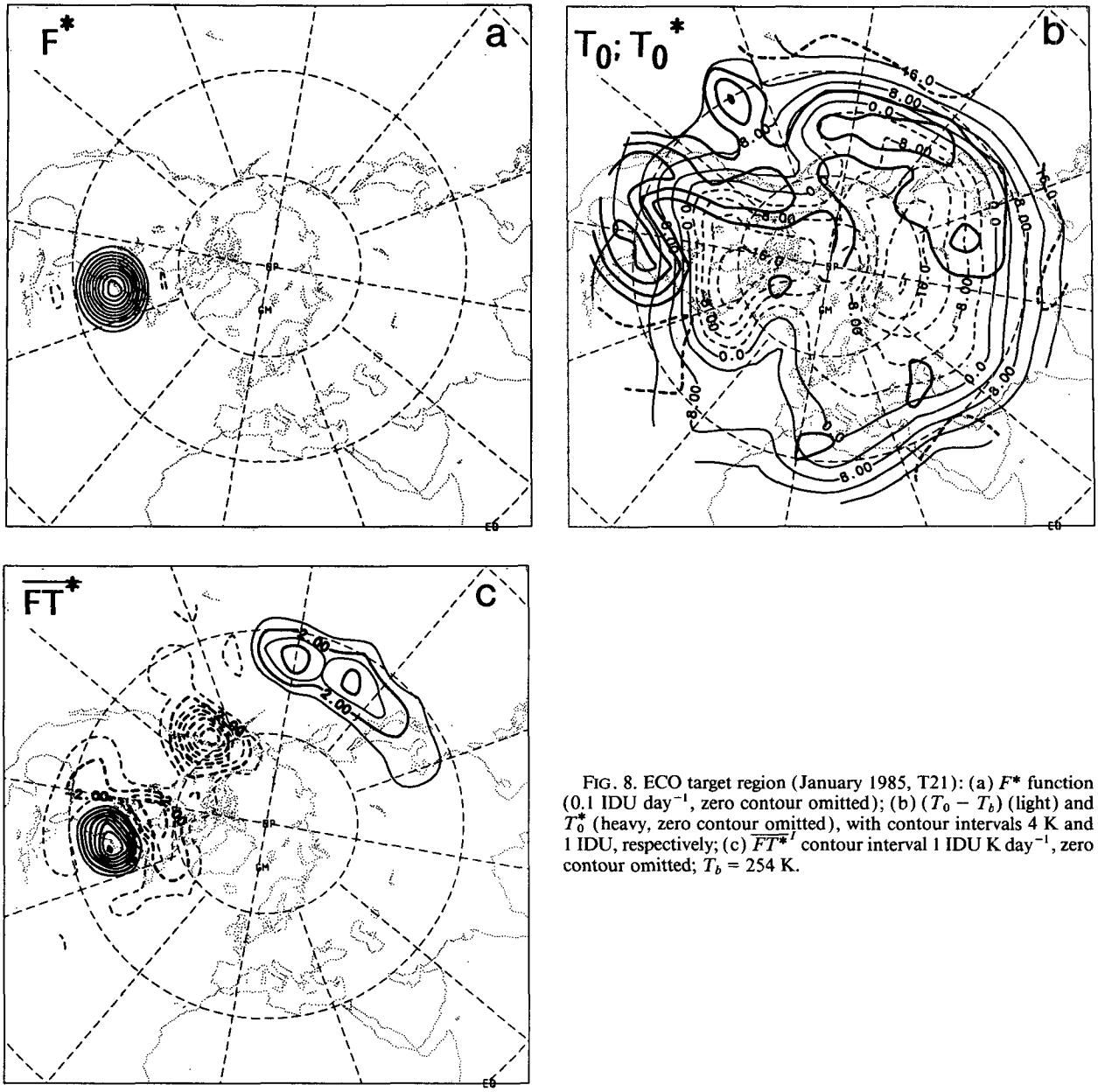

FIG. 8. ECO target region (January 1985, T21): (a) F^* function (0.1 IDU day^{-1}, zero contour omitted); (b) $(T_0 - T_b)$ (light) and T_0^* (heavy, zero contour omitted), with contour intervals 4 K and 1 IDU, respectively; (c) $\overline{FT^*}^I$ contour interval 1 IDU K day^{-1}, zero contour omitted; T_b = 254 K.

matological choice of T_b dictates that the ICs must trivially balance this cooling. Thus, the division of the regional anomaly into IC and forcing components loses its meaning in the climatological mean, unless T_b can be alternatively specified (e.g., as some *other* climatological temperature). On the other hand, the climatological T_b enables individual January anomalies to be defined. Large January temperature anomalies (>2 K) occurred in 1983 and 1985, and in both cases over 80% of the anomaly amplitude can be expressed in terms of anomalies in the ICs. The IC anomalies exhibit more variance than the forcing anomalies, while the latter often play a large role in weaker temperature anomalies. Thus, it appears that (for the small sample of six Januarys) one month is too short to produce large-amplitude anomalies in the forcing, and that large regional anomalies are primarily the result of advection of preexisting air masses.

Figure 9 illustrates the spatial fields associated with the six-January average. The climatological ICs have a rather zonal structure, with relatively warm air to the south, especially over the oceans, and colder air over the polar regions. The forcing effects indicate that a net cooling over Canada and Europe itself dominates

TABLE 6. Values of terms in (12) in kelvin for six Januarys (central Europe): Six-January mean and deviations from that mean. $T_b = 251$ K. The last column contains the ratio of forcing to ICs deviations.

January	Anomaly $\overline{T}^{G,I}$	ICs $\int_H (T_0 - T_b)T_0^*$	Forcing $\int_H \int_I T^*F$	Forcing/ICs
		Six-January mean		
	+0.03	+2.03	−2.00	
		Deviations		
1980	−1.22	−0.42	−0.81	+1.93
1981	−0.77	−0.51	−0.26	+0.51
1982	+1.26	+0.38	+0.88	+2.31
1983	+2.70	+3.02	−0.32	−0.11
1984	+0.67	−0.29	+0.96	−3.31
1985	−2.63	−2.18	−0.45	+0.21

over net warming over the Atlantic. Note how Fig. 9c (the *effects* of net heating on central Europe) differs from the distribution of $\hat{F}$ in Fig. 4a through the weighting function T^*, which has a maximum over the target area (not shown). Clearly, a small cooling here has a relatively large effect on the temperature budget of the region, and one must be aware of model deficiencies here.

Figure 10 illustrates the spatial fields for January 1983, the warmest month, which may be contrasted with January 1985, the coldest month in Fig. 5. The T_0^* field (Fig. 10a) suggests a zonal regime, and traces the "advective" part of the anomaly (the main component according to Table 6) back to preexisting warm air masses over the Atlantic, especially the Gulf of Mexico, and even the west Pacific. Because of the zonal nature of the month, the $(T_0 - T_b)T_0^*$ field in Fig. 10b is weak in amplitude compared with the January 1985 case. Subtracting the climatological ICs (Fig. 9b) would yield the *anomalous* ICs (not shown), whose spatial integrals appear in Table 6.

Figure 10c presents an anomaly map of the net heating effects on the target region for January 1983, that is, the deviation from the climatology in Fig. 9c. Anomalously large local heating over the target region is offset by anomalously small heating over the Atlantic to give the small negative anomaly in Table 6. (Note that Fig. 10c is an anomaly map, so that a direct comparison with the 1985 case in Fig. 5c is not possible.)

As discussed in section 6, the thermodynamic sources implied as a residual from (1) contain substantial adiabatic heating effects associated with vertical motions, precluding a direct interpretation in terms of diabatic effects. However, an estimation of the roles of diabatic and adiabatic effects on the European January anomalies may be made using the quasigeostrophic theory introduced in section 5. To this end, we have split the forcing integrals in Table 6 into their components via (13) and listed the results in Table 7.

The effect of vertical motions on the six-January average temperature over the target region considerably exceeds the residual diabatic effects. According to these rather crude estimates, the negative climatological net forcing is a result of adiabatic cooling dominating over diabatic heating and a positive cross-correlation term. Figure 11 illustrates the spatial distributions of $S_p(\widehat{\omega T^*})^I$ and $\widehat{QT^*}^I$ (i.e., the six-January grand means). Climatological adiabatic effects on the target region are mostly negative, while the diabatic effects are strongly positive over the Atlantic. The distribution of the climatological *net* forcing effects, $\widehat{FT^*}^I$, in Fig. 9c is approximately given by the local dominance of one effect over the other (neglecting the cross-correlation term).

Deviations from the six-January mean also show large cancellations between the adiabatic and (residual) diabatic effects, with a smaller net effect in most cases. The cross-correlation term is generally secondary, except in January 1982 and 1985. Figure 12 illustrates the spatial fields of the *anomalies* in the adiabatic and diabatic components for January 1983 and 1985. In January 1983 there is a good anticorrelation in many locations between adiabatic temperature changes associated with vertical motions and the residual diabatic effects, while horizontal advection (and model errors) plays a more important role during January 1985. Figure 13 shows the 500-mb geopotential height anomalies for January 1983 and 1985 (panels a and b), and the associated anomalies in bandpass (2.5–6-day period) rms height (panels c and d). In January 1983 there is an anomalous ridge centered over southwest Europe and the storm track is enhanced around its northern and eastern flank, extending into the eastern Mediterranean. In contrast, the 500-mb geopotential height anomaly in January 1985 is almost the reverse, with a blocking dipole signature over the east Atlantic, with the storm track enhanced to the west and south.

According to the adjoint diagnosis, the largest part of the associated temperature anomalies over central Europe (warm ridge, cold block) may be traced back to air masses (with very different origins) present at the beginning of the months. The much smaller (in both cases negative) anomalous thermodynamic effects appear to be associated with the dominance of anomalous adiabatic cooling over diabatic heating, accompanying deviations in the storm tracks. The anomalous adiabatic heating effects and implied diabatic effects (Table 7) are much larger in January 1983 than in January 1985, suggesting faster energy transfer associated with the rapid passage of cyclones in January 1983.

8. Discussion

We have demonstrated how the adjoint method can be used to quantify regional temperature anomalies in terms of horizontal advection and thermodynamic source terms using a one-layer model. Once-daily ob-

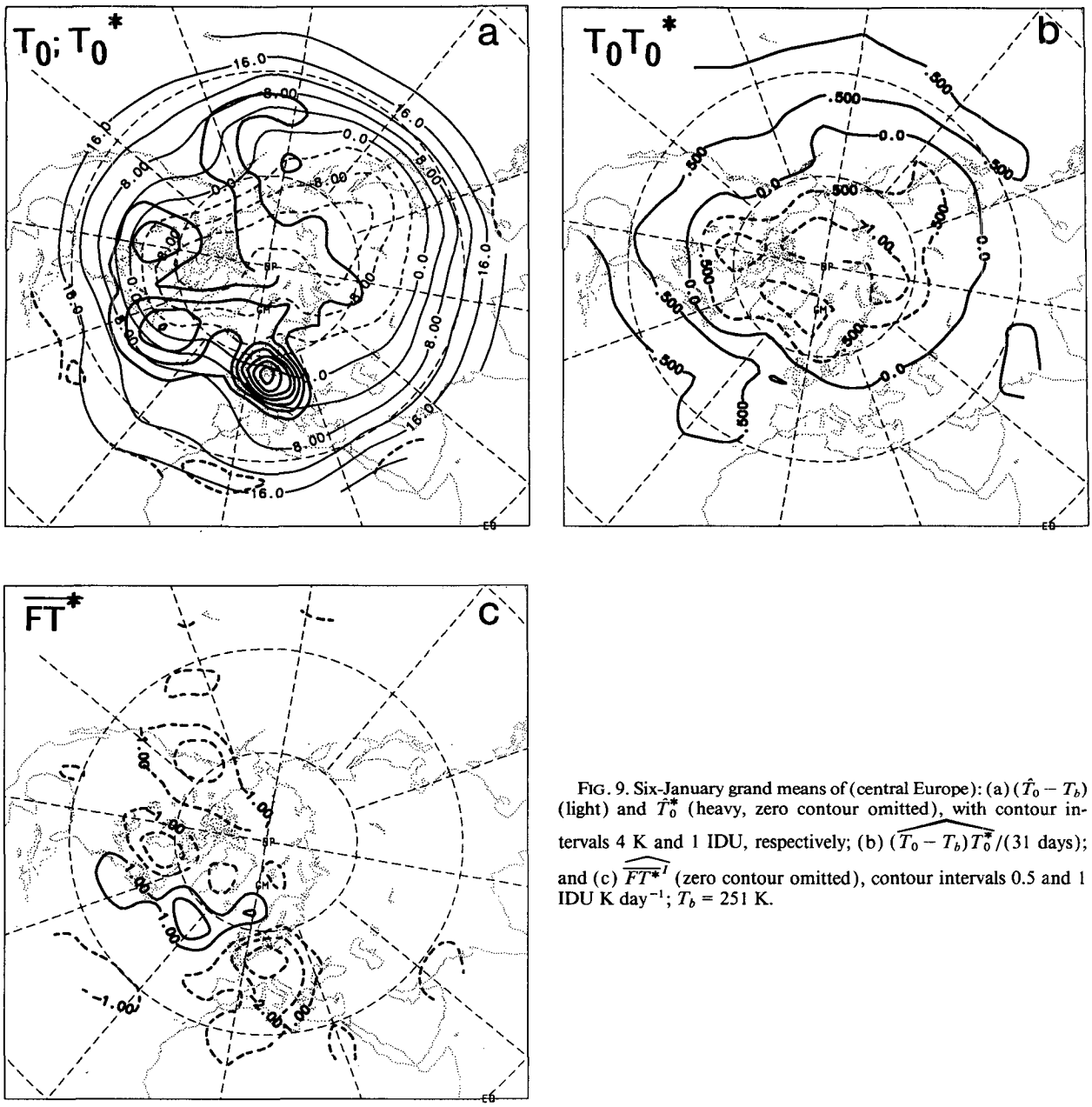

FIG. 9. Six-January grand means of (central Europe): (a) $(\hat{T}_0 - T_b)$ (light) and $\hat{T}_0^*$ (heavy, zero contour omitted), with contour intervals 4 K and 1 IDU, respectively; (b) $\widehat{(T_0 - T_b)T_0^*}/(31 \text{ days})$; and (c) $\widehat{FT^{*I}}$ (zero contour omitted), contour intervals 0.5 and 1 IDU K day^{-1}; $T_b = 251$ K.

served hemispheric data provides sufficient information to enable the unforced (temperature) tracer equation to be integrated forward in time. Furthermore, simulated tropospheric averages of temperature are still recognizable after 28 days of integration, with the phases of the temperature waves caught quite well, so that the one-layer model would appear to be suitable for discussing regional temperature anomalies. However, a considerable cancellation between diabatic forcing and adiabatic forcing associated with vertical motions is probably partly responsible for the success of the unforced model.

In the tropospheric average, the concept of the "advective limit" turns out to be inadequate, and the residual forcing deduced from the one-layer model must be interpreted in terms of diabatic effects together with compensating adiabatic temperature changes associated with vertical motions. Palmer and Sun (1985) suggest that in middle latitudes vertical motions can play an important role in compensating for diabatic effects (from a diagnostic point of view), if there is cancellation between meridional and zonal advection of temperature. In our tropospheric average case, it was found that in the six-January mean there is indeed

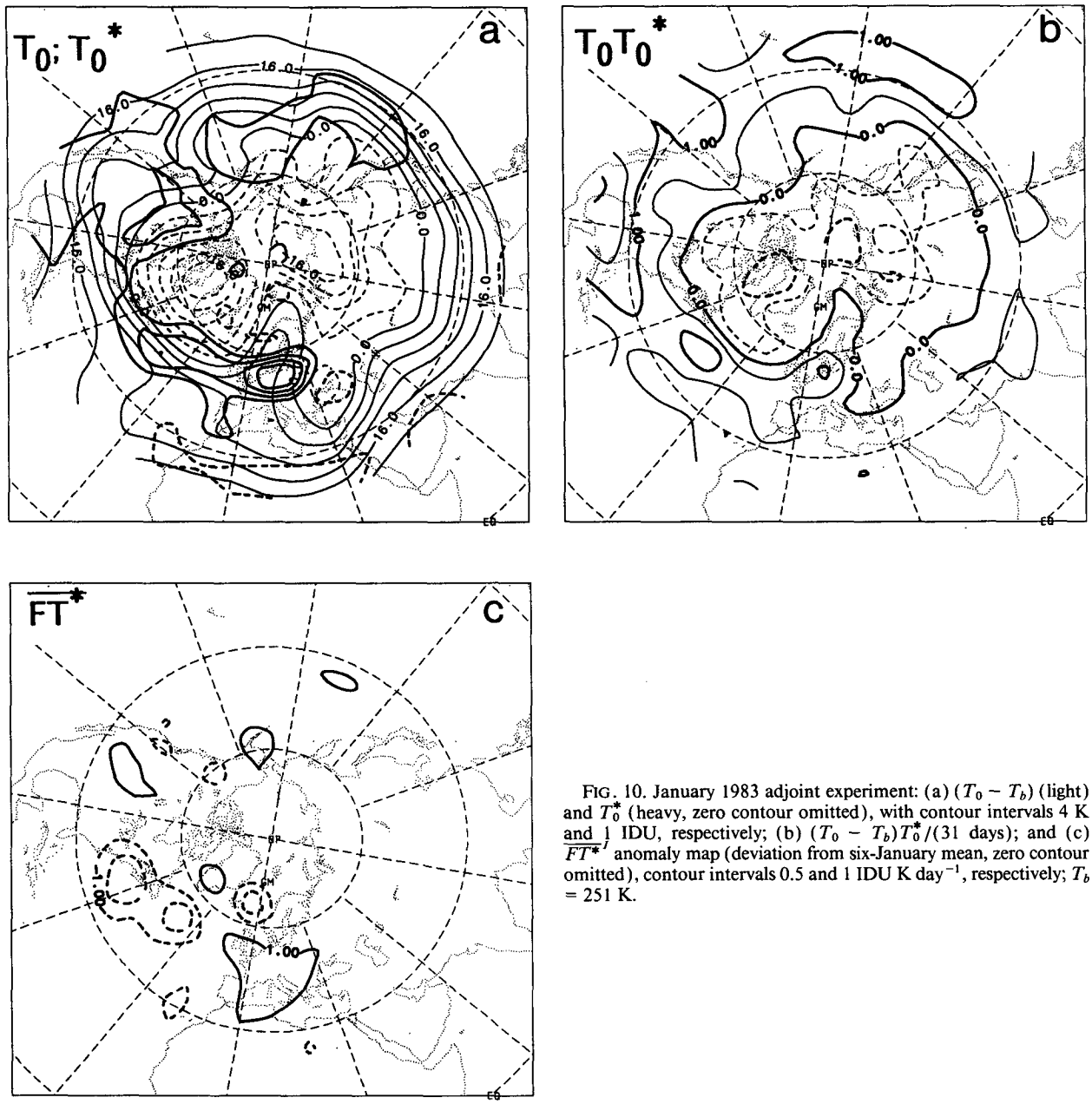

FIG. 10. January 1983 adjoint experiment: (a) $(T_0 - T_b)$ (light) and T_0^* (heavy, zero contour omitted), with contour intervals 4 K and 1 IDU, respectively; (b) $(T_0 - T_b)T_0^*/(31$ days); and (c) $\overline{FT^*}'$ anomaly map (deviation from six-January mean, zero contour omitted), contour intervals 0.5 and 1 IDU K day^{-1}, respectively; T_b = 251 K.

very substantial cancellation between these two terms, so that their residual is of the same order as the vertical-motion term. Zonal cold advection dominates over poleward warm advection over the eastern continents, giving the dominant signature in Fig. 4a. Hense et al. (1990) have found the "advective limit" to be a useful approximation for discussing the influence of midlatitude sea surface temperature anomalies at low levels, and in the tropospheric average, we may well be mixing together different balances at different levels. Application of the adjoint method to the 850–1000-mb layer did not, however, yield a useful result.

The tropospheric-averaged quasigeostrophic analysis suggests that diabatic heat sources and sinks are usually accompanied by substantial compensating vertical motions. However, the net heating may have a more fundamental significance than the diabatic heating itself in a one-layer model. This net heating is a function of the flow, and its magnitude measures the extent to which the equivalent barotropic component of the flow diverges from free-mode form. We note that even the diabatic heating is generally a function of the flow if there is a degree of thermal equilibration, as discussed by Marshall and So (1990).

TABLE 7. Components of forcing term in (12) in kelvin using (13) for 6 Januarys (central Europe): Six-January mean and deviations from that mean. $S_p = 0.06$ K mb^{-1}.

January	Forcing $\iint T^*F$	Adiabatic $S_p \iint T^*\langle\omega\rangle$	Cross correlation $-\iint T^*\langle v'\cdot\nabla T'\rangle$	Diabatic $\iint T^*\langle Q\rangle$
		Six-January mean:		
	−2.00	−4.30	+1.08	+1.22
		Deviations:		
1980	−0.81	+2.29	+0.22	−3.32
1981	−0.26	+0.55	+0.07	−0.88
1982	+0.88	+0.88	+0.31	−0.30
1983	−0.32	−1.84	+0.02	+1.48
1984	+0.96	−1.39	−0.31	+2.66
1985	−0.45	−0.50	−0.32	+0.37

The adjoint method divides the roots of regional temperature averaged over a given period into two components: a preexisting distribution, which is simply advected, and thermodynamic sources and sinks occurring within the period, whose effects are then also advected into the region. The longer the period, the greater the impact of the thermodynamic sources and sinks. Our large monthly temperature anomalies were primarily accounted for by anomalies in the initial conditions, though this ought to be less the case if seasonal anomalies were considered. Crudely speaking, the air trajectory remembers its starting temperature up to the diabatic time scale (~10 days: taking $|Q| \sim 1$ K day^{-1} and $|\Delta T| \sim 10$ K). The advective time scale is an Eulerian concept and is thus not directly applicable. Nevertheless, the time that a trajectory spends in a heating region determines the heating it experiences, and if it traverses alternating regions of heating and cooling, its heating history is characterized by a lot of cancellation, as seen in Fig. 9c. The experiments with different target regions emphasize that the method diagnoses a regional anomaly in terms of its (upstream) advective "influence" region, whose extent depends on the speed of the flow. A mean advection speed of 10 m s^{-1} gives an extent of ~10 000 km (or 140° of longitude at 50°N) over a diabatic time scale of ~10 days. Thus, the effect of the Pacific storm track is directly felt by the east coast of North America in January 1985, but not by Europe. The effects of upstream events are communicated by advection and are increasingly lost over large distances as the time interval approaches the diabatic time scale, despite the insensitivity of the model to suppressing the dissipation.

Although anomalous forcing effects played a secondary role in accounting for six January central European anomalies, it is possible that the indirect effect of the forcing (via associated flow changes) is much greater. While such indirect effects cannot be studied with a tracer model alone, a linear wave model could be used to compute the flow response associated with forcing, whose advection could then be examined with the adjoint tracer model. Further work is also required to develop a true anomaly formulation, to enable anomalous advection to be distinguished from anomalies in diabatic processes and anomalies in the temperature distribution at the start of the period.

According to the adjoint diagnosis, the central European temperature in the six-January mean is associated with net cooling, especially over Europe itself

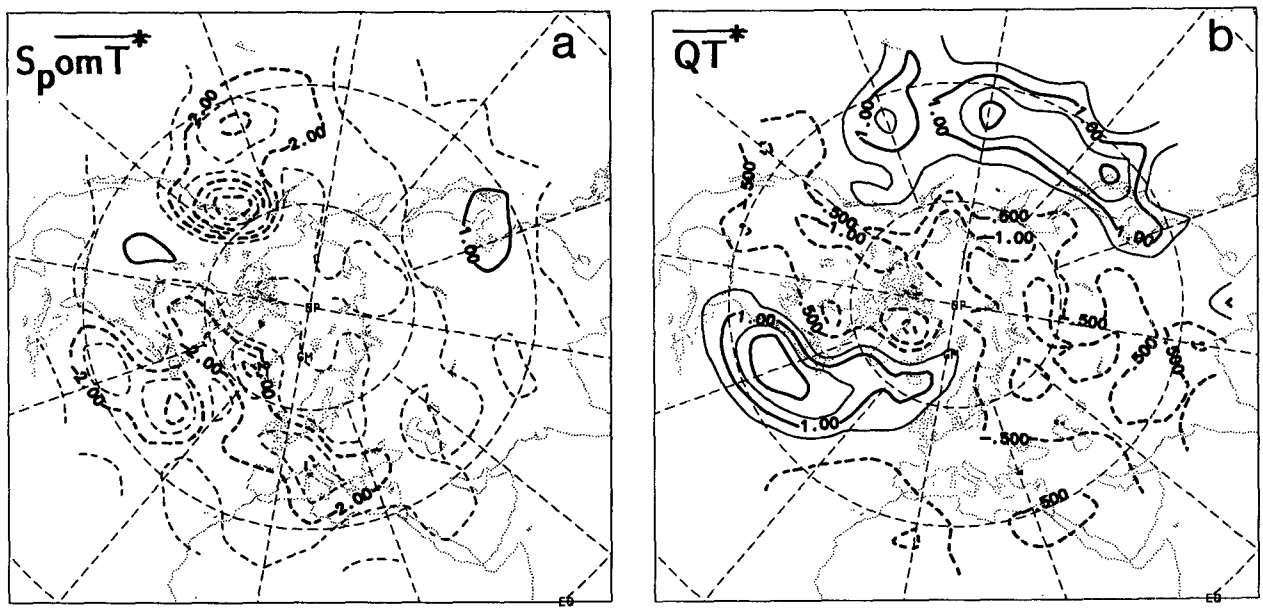

FIG. 11. Six-January mean heating effects: (a) $\widehat{S_p\overline{\omega T^*}^{1}}$ and (b) $\widehat{\overline{QT^*}^{1}}$; contour interval 1 IDU K day^{-1}, zero contour omitted.

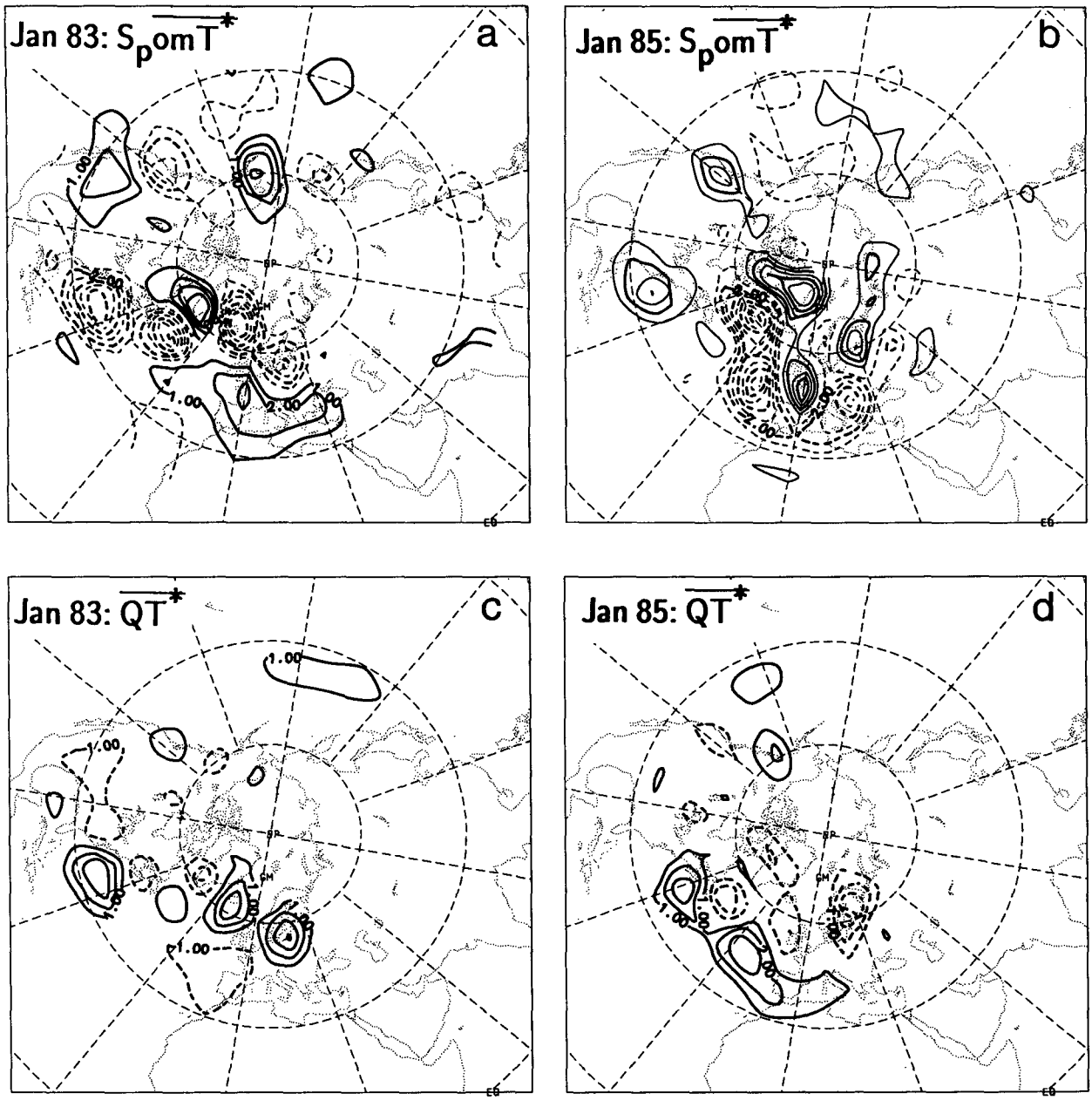

FIG. 12. Anomalous heating effects for January 1983 and 1985: (a) and (b) $S_p\overline{\omega T^*}'$ anomaly and (c) and (d) $\overline{QT^*}'$ anomaly; contour interval 1 IDU K day^{-1}, zero contour omitted.

and over North America, which is partially offset by net heating over the Atlantic. This diagnosis could be repeated on "control" and "response-experiment" climates of a GCM, to explore changes in the regional temperature budget associated with global climate change. For example, one could repeat section 7 with all GCM Januarys and simply consider the difference between control and response climates. Such a study is under way. The use of a dynamically consistent and complete GCM dataset would additionally enable the diabatic effects on regional anomalies to be explicitly calculated.

The adjoint method also has scope for investigating persistent anomalies on the time scale of weeks. Indeed, while in the individual Januarys studied some consistency was found between deviations in the position of the Atlantic storm track and anomalies in the components of the thermodynamic forcing, dynamically coherent weather regimes would form an ideal basis for such an investigation, rather than calendar months.

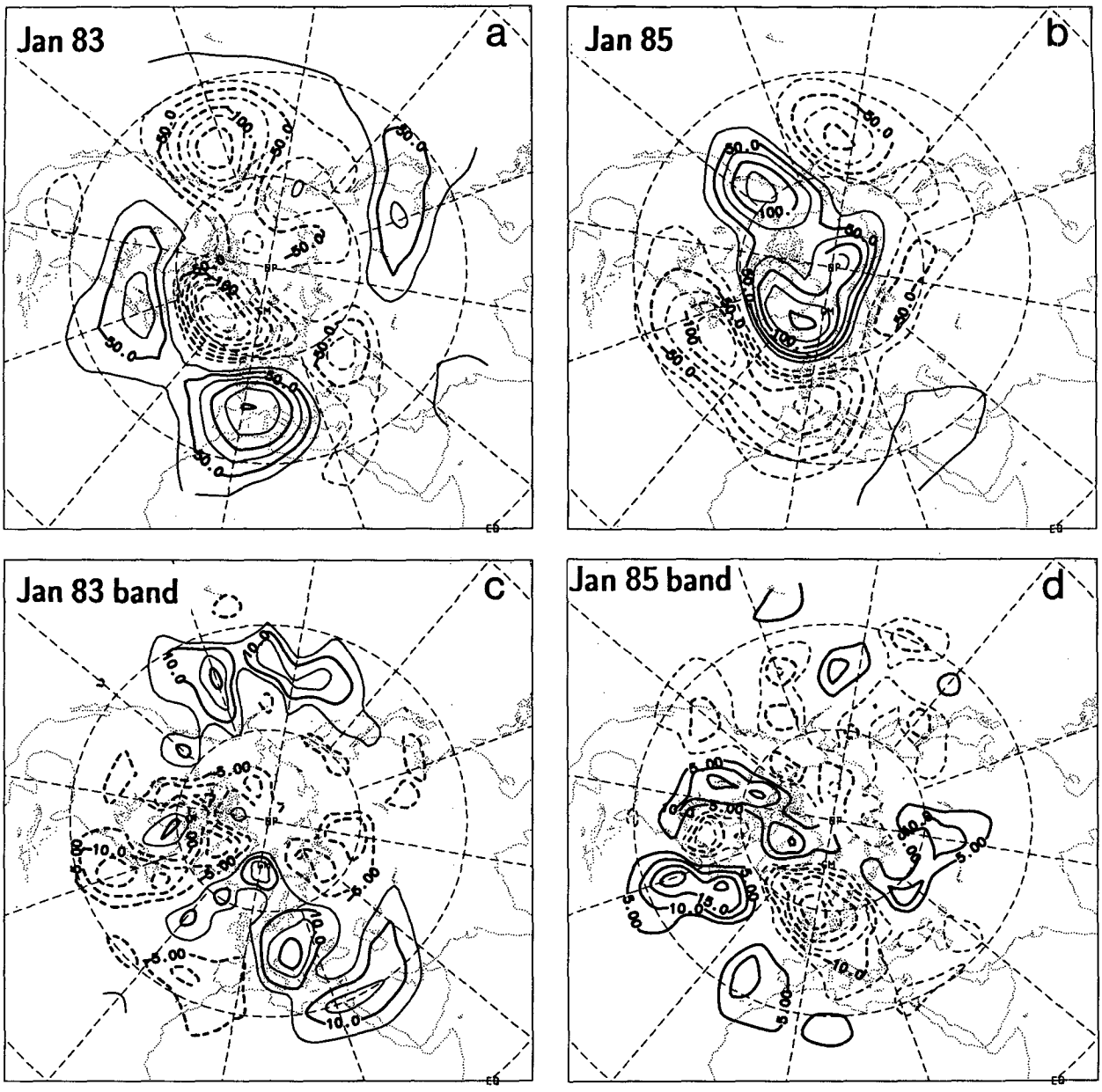

FIG. 13. Observed 500-mb geopotential height anomalies (with respect to the six-January mean) for January (a) 1983 (left) and (b) 1985 (right), contour interval 25 gpm. Parts (c) and (d): the respective anomalies in rms bandpass-filtered 500-mb height, contour interval 5 gpm; zero contour omitted.

Acknowledgments. I am indebted to J. Egger for suggesting the adjoint method as a diagnostic tool. I thank M. Blackburn, J. Egger, W. Metz, and F. Schmidt for reading earlier versions of the manuscript and making many valuable suggestions. This work was supported by the Bavarian climate program (Bay FORKLIM).

APPENDIX

The Discretized Adjoint Problem

In order to evaluate the contributions of the initial conditions and forcing to a time-averaged regional temperature anomaly by means of (12), it is necessary to derive a discretized analog of (12) consistent with the discretized analogs of (1) and (3).

We define the discretized inner product of two hemispheric temperature fields over a time interval $\Delta t = t_N - t_0$ to be

$$\langle T, T' \rangle = \sqrt{2}\pi \frac{\Delta t}{N+1} \sum_{t=0}^{N} [(TT')]_t,$$

$$= \sqrt{2}\pi \Delta t \overline{[TT']}^I, \qquad \text{(A1)}$$

where $[TT']$ denotes the $(m = 0, n = 0)$ spherical

harmonic coefficient of the product between the hemispheric fields T and T' computed in gridpoint space, and the sum is over a set of $N+1$ discrete times. The product is computed on a Guassian grid such that there is no aliasing of the resolved spectral components. In practice, the discrete times and the Gaussian grid are those used in the integration of (3). The inner product defined by (A1) is simply the time mean of the (0, 0) spectral component of the usual scalar product of the two fields.

Equation (10) is formed by taking the inner products of (1) with T^* and (3) with T, respectively, and subtracting the second product from the first:

$$\langle T^*, \partial T/\partial t\rangle + \langle T, \partial T^*/\partial t\rangle + \langle T^*, \mathbf{v}\cdot\nabla T\rangle + \langle T, \mathbf{v}\cdot\nabla T^*\rangle + \langle T, \kappa\nabla^4 T^*\rangle - \langle T^*, \kappa\nabla^4 T\rangle = \langle T^*, F\rangle - \langle F^*, T\rangle.$$

The advection terms give

$$\langle T^*, \mathbf{v}\cdot\nabla T\rangle + \langle T, \mathbf{v}\cdot\nabla T^*\rangle = \sqrt{2}\pi\Delta t[\overline{\nabla\cdot(TT^*\mathbf{v}) - (TT^*\nabla\cdot\mathbf{v} + T\mathbf{v}\cdot\nabla T^* + T\mathbf{v}\cdot\nabla T^*)}^I = \sqrt{2}\pi\Delta t[\overline{\nabla\cdot(TT^*\mathbf{v})}]^I = 0,$$

with periodic boundary conditions, as in the continuous case.

Consider now the discrete analogs of the tendency terms, with the leapfrog scheme and Euler time steps at $t = t_N$ and t_0 in both (1) and (3)

$$\langle T^*, \partial T/\partial t\rangle + \langle T, \partial T^*/\partial t\rangle = \sqrt{2}\pi\frac{\Delta t}{N+1} \times \sum_{t=0}^{N}[T_t^*(T_{t+1} - T_{t-1})/2\Delta t' + T_t(T_{t+1}^* - T_{t-1}^*)2/\Delta t'],$$

where

$$T_{-1} = 2T_0 - T_1$$

$$T_{N+1} = 2T_N - T_{N-1} = \frac{\sqrt{2}\pi\Delta t}{(N+1)2\Delta t'} \times [-4T_0^* T_0 + (T_0^* T_1 + T_0 T_1^*) - T_N T_{N-1}^*],$$

using the initial condition $T_N^* = 0$, where $\Delta t'$ is the time step.

The diffusion terms applied at time step "$t-1$" with leapfrog but at time t for the initial/final Euler steps yield, for ∇^4 diffusion:

$$\langle T, \kappa\nabla^4 T^*\rangle - \langle T^*, \kappa\nabla^4 T\rangle = \sqrt{2}\pi\kappa\frac{\Delta t}{N+1}\sum_{t=0}^{N}[T_t\nabla^4 T_{t+1}^* - T_t^*\nabla^4 T_{t-1}] = \sqrt{2}\pi\kappa\frac{\Delta t}{N+1}\sum_{t=0}^{N}[\nabla^2 T_t\nabla^2 T_{t+1}^* - \nabla^2 T_t^*\nabla^2 T_{t-1}] = -\sqrt{2}\pi\kappa\frac{\Delta t}{N+1}[\nabla^2 T_1^*\nabla^2 T_0],$$

again making use of $T_N^* = 0$ and $[\nabla\cdot(\ )] = 0$.

Neglecting this residual diffusion term, which is very small for large N, we arrive at the following discretized analog of (10):

$$\Delta t\overline{[F^*T]}^I = \frac{N}{(N+1)}\frac{1}{2}[4T_0^* T_0 - (T_0^* T_1 + T_0 T_1^*) - T_N T_{N-1}^*] + \Delta t\overline{[T^*F]}^I,$$

from which (12) follows. In fact, the first term in square brackets on the rhs, the initial-conditions term, is very nearly equal to $T_0^* T_0$ with a 1-h time step, since $T_N^* = 0$.

REFERENCES

Grotch, S. L., and M. C. MacCracken, 1991: The use of general circulation models to predict regional climate change. *J. Climate,* **4,** 286–303.

Hense, A., R. Glowienka-Hense, H. von Storch, and U. Stähler, 1990: Northern Hemisphere atmospheric response to changes of Atlantic Ocean SST on decadal time scales: A GCM experiment. *Climate Dyn.,* **4,** 157–174.

Holton, J. R., 1979: *An Introduction to Dynamical Meteorology.* Academic Press, 391 pp.

Hoskins, B. J., and D. J. Karoly, 1981: The steady linear response of a spherical atmosphere to thermal and orographic forcing. *J. Atmos. Sci.,* **38,** 1179–1196.

——, H. H. Hsu, I. N. James, M. Masutani, P. D. Sardeshmukh, and G. H. White, 1989: Diagnostics of the global atmospheric circulation based on ECMWF analyses 1979–89. World Climate Research Program Report No. 27, WMO/TD-No. 326, 217 pp.

Kontarev, G., 1980: The adjoint equation technique applied to meteorological problems. ECMWF Tech. Rep. No. 21, 21 pp.

Lanczos, C., 1961: *Linear Differential Operators.* D. van Nostrand, 564 pp.

Marchuk, G. I., 1974: *Numerical Solutions of Problems in Atmospheric and Oceanic Dynamics.* Gidrometeoizdat Press, (in Russian).

——, and Y. N. Skiba, 1976: Numerical calculation of the conjugate problem for a model of the thermal interaction of the atmosphere with the oceans and continents. *Izv., Atmos. Oceanic Phys.,* **12,** 279–284.

Marshall, J., and D. W. K., So, 1990: Thermal equilibrium of planetary waves. *J. Atmos Sci.,* **47,** 963–978.

Palmer, T. N., and Z. Sun, 1985: A modelling and observational study of the relationship between sea surface temperature in the northwest Atlantic and the atmospheric general circulation. *Quart. J. Roy. Meteor. Soc.,* **111,** 947–975.

Smagorinsky, J., 1953: The dynamical influence of large-scale heat sources and sinks on the quasi-stationary mean motions of the atmosphere. *Quart J. Roy. Meteor. Soc.,* **79,** 342–366.

Talagrand, O., and P. Courtier, 1987: Variational assimilation of meteorological observations with the adjoint vorticity equation. Part 1: Theory. *Quart J. Roy. Meteor. Soc.,* **113,** 1311–1329.